Supporting Information for "Enhanced widefield quantum sensing with nitrogen-vacancy ensembles using diamond nanopillar arrays"

Daniel J. McCloskey,[*,†] Nikolai Dontschuk,[†,‡] David A. Broadway,[†,‡] Athavan Nadarajah,[†] Alastair Stacey,[†,‡] Jean-Philippe Tetienne,[†] Lloyd C. L. Hollenberg,[†,‡] Steven Prawer,[†] and David A. Simpson[*,†]

†*School of Physics, University of Melbourne, Parkville, VIC 3010, Australia*

‡*Centre for Quantum Computation and Communication Technology, University of Melbourne, Parkville, VIC 3010, Australia*

E-mail: dmccloskey@student.unimelb.edu.au; simd@unimelb.edu.au

Nanopillar Array Fabrication

The fabrication pathway for the diamond pillar arrays as described in the experimental section of the main text is sketched in Figure S1.

Contrast and Sensitivity Increases

We observed a correlation between the highest ODMR contrast achievable on a single family of NV centres with the contribution to the PL spectrum from the negatively-charged NV

centre (NV^-). For clarity, we plot these data alongside each other here (Figure S2a). Using equation 1 in the main text, the increase in ODMR imaging sensitivity offered by the pillars over the flat surface is computed simply as $C_{boost}\sqrt{\epsilon_{boost}T^*_{2boost}}$, where $C_{boost} = \frac{C_{pillar}}{C_{flat}}$ is the measured ODMR contrast improvement, $\epsilon_{boost} = \frac{\epsilon_{pillar}}{\epsilon_{flat}}$ is the measured increase in photon count rate and $T^*_{2boost} = \frac{T^*_{2pillar}}{T^*_{2flat}}$ is the measured increase in T_2* for each pillar tip diameter. The sensitivity increases and associated experimental uncertainties are shown in Figure S2b.

Stress Maps of the Unpatterned Surface

ODMR spectral images of the unpatterned surface were taken under the same conditions (ie. same external magnetic field, number of integrations, Rabi frequencies) as the images of the pillar arrays shown in the main text. The PL image of this area is shown in Figure S3a, while the resulting stress maps are shown in Figure S3b-e. Standard deviations were computed across the images in order to assess the noise floor of the measurements. The obtained values are given in Figure 4 of the main text. Note that the large gradient in the map of axial stress (Figure S3b) was subtracted prior to the calculation of the standard deviation in σ_{axial}.

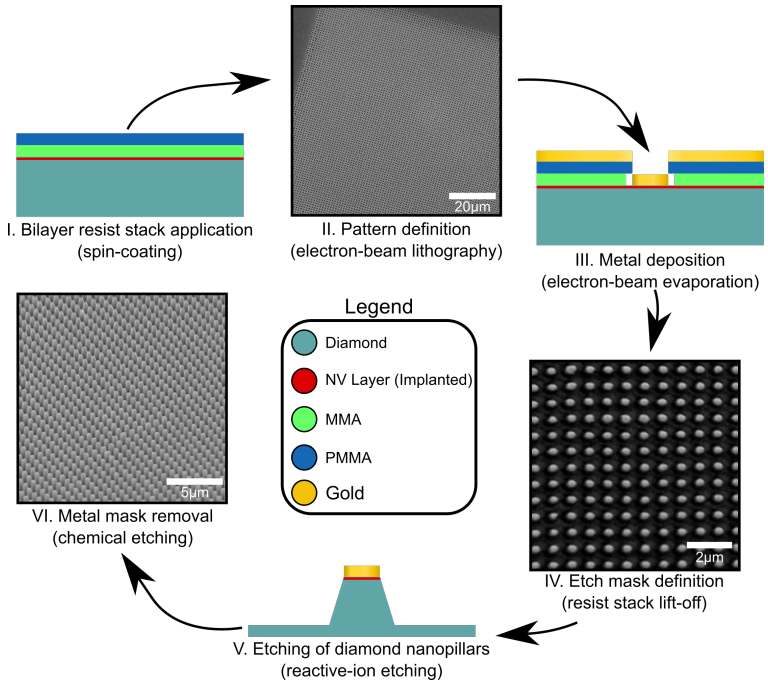

Figure S1: Nanopillar array fabrication. i) Application of MMA/PMMA bilayer stack by spin-coating. ii) Electron-beam lithography exposure and development of the array pattern. iii) Electron-beam evaporation of Cr/Au etch-masks. iv) Liftoff of remaining unexposed resist in acetone. v) Reactive-ion etching of tapered diamond nanopillars. vi) Wet chemical etching of remaining Cr/Au. Pictured pillars have a nominal tip diameter of 400 nm and an array pitch of 800 nm.

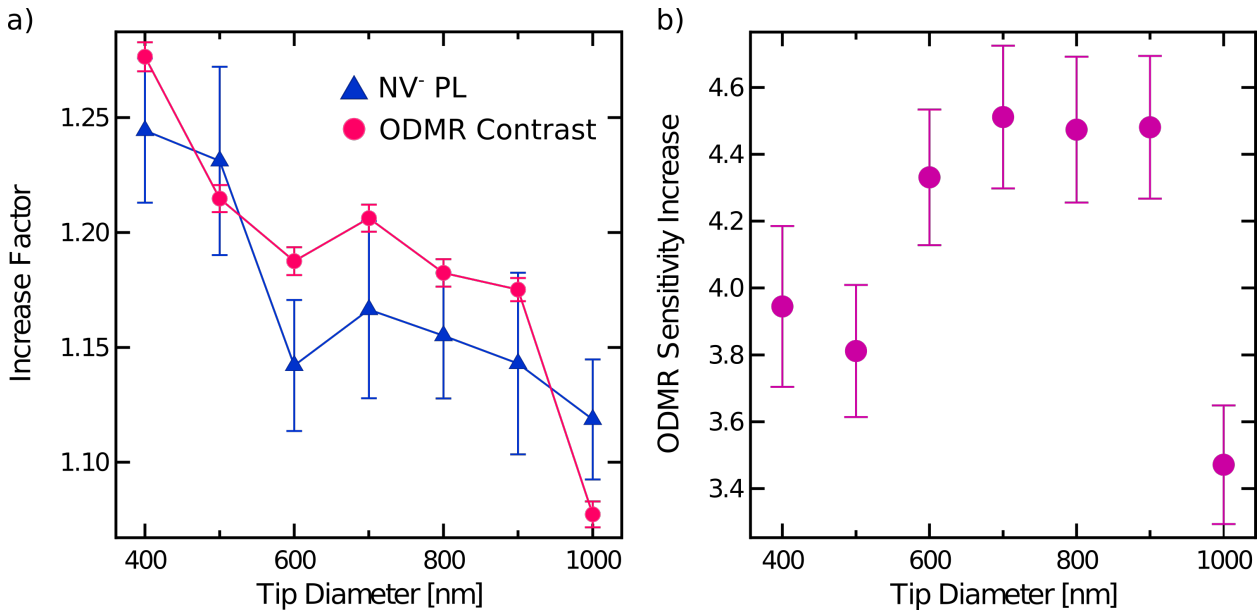

Figure S2: Improvements in ODMR contrast and total imaging sensitivity. a) Correlated relative increases in maximal single-family ODMR contrast and PL from NV^- as a function of pillar tip diameter. b) Predicted improvements in ODMR imaging sensitivity of diamond nanopillar arrays, accounting for measured increases in photon collection, intrinsic coherence time T_2*, and ODMR contrast. Error bars are quadrature sums of uncertainties in the aforementioned values.

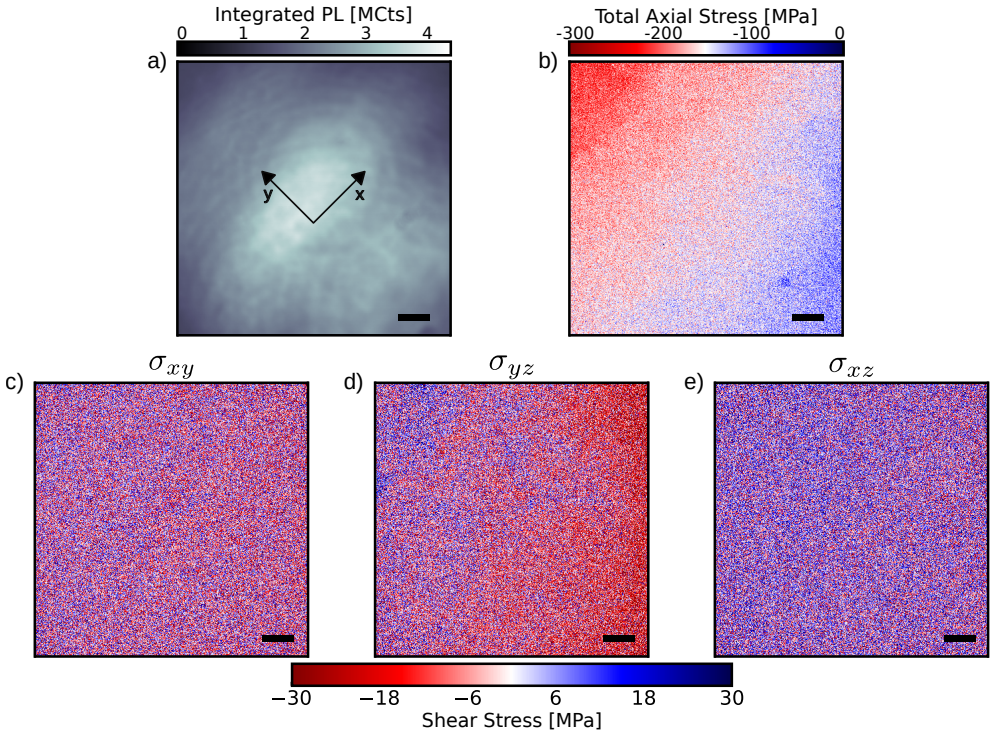

Figure S3: Mechanical stress maps of unpatterned diamond surface. a) Photoluminescence image of the region studied and the xy coordinate system used to define the stress tensor components. b) Map of total axial stress of the region shown in (a). The gradient across the image is a result of PL variation, and was subtracted prior to calculating the standard deviation in the measurement. c), d), e) Maps of shear stress tensor components σ_{xy}, σ_{yz}, and σ_{xz} respectively. Scale bars are 10 µm.